X-ray fluorescence study of organic-inorganic polymer conversion into ceramics induced by ion irradiation

メタデータ	言語: eng
	出版者:
	公開日: 2017-10-03
	キーワード (Ja):
	キーワード (En):
	作成者:
	メールアドレス:
	所属:
URL	https://doi.org/10.24517/00010105

This work is licensed under a Creative Commons Attribution-NonCommercial-ShareAlike 3.0 International License.

PHYSICAL REVIEW B VOLUME 60, NUMBER 22 1 DECEMBER 1999-II

X-ray fluorescence study of organic-inorganic polymer conversion into ceramics induced by ion irradiation

E. Z. Kurmaev
Institute of Metal Physics, Russian Academy of Sciences–Ural Division, 620219 Yekaterinburg GSP-170, Russia

A. Moewes
CAMD, Louisiana State University, 6980 Jefferson Highway, Baton Rouge, Louisiana 70806

M. Krietemeyer
Department of Physics, University of Osnabruck, Osnabruck, D-49069, Germany

K. Endo, T. Ida, and S. Shimada
Department of Chemistry, Faculty of Science, Kanazawa University, Kanazawa, Japan

R. P. Winarski
Department of Physics, Tulane University, New Orleans, Louisiana 70118

M. Neumann
Department of Physics, University of Osnabruck, Osnabruck, D-49069, Germany

S. N. Shamin
Institute of Metal Physics, Russian Academy of Sciences–Ural Division, 620219 Yekaterinburg GSP-170, Russia

D. L. Ederer
Department of Physics, Tulane University, New Orleans, Louisiana 70118
(Received 29 June 1999)

Changes to the local and electronic structures of phenyltriethoxysilane (PTES) films when irradiated at room temperature with gold ion concentrations of 5×10^{14} to $2.5\times10^{15}\,\mathrm{cm}^{-2}$ and with carbon ion concentrations of $5\times10^{15}\,\mathrm{cm}^{-2}$ were studied using x-ray emission and photoelectron spectroscopies. The fluorescent ultrasoft silicon $L_{\mathrm{II,III}}$ and carbon $K\alpha$ x-ray emission spectra of unirradiated and irradiated PTES films were measured at the Advanced Light Source, and the Center for Advanced Microstructures and Devices. It is found that the PTES polymers that are exposed to ion doses higher than $5\times10^{14}\,\mathrm{cm}^{-2}$ convert to Si:O:C ceramics. Annealing the irradiated PTES polymer films at 1000 °C segregates the carbon atoms into sp^2-like clusters.
[S0163-1829(99)00546-9]

I. INTRODUCTION

Preparation of ceramic coatings by the pyrolitic conversion of alkoxide gels or organic-inorganic polymers is considered a versatile and economical means of homogeneously depositing precursors from solutions on irregular surfaces.[1] However, the synthesis of carbide films (SiC, SiOC) by polymer pyrolysis has not been pursued[2] due to the high temperature (about 1000–1400 °C) treatments necessary for removing most of the hydrogen from the silicon carbide and oxycarbide precursors possessing high stability single C-H bonds. It was recently shown that ion irradiation can be used to prepare ceramic coatings from polymer precursors as it provides for a complete release of hydrogen at room temperature.[3]

In this paper we have investigated the chemical reactions in phenyltriethoxysilane (PTES) polymer films induced by irradiation with gold and carbon ions using ultrasoft x-ray fluorescence measurements. We recently showed (Refs. 4–7) that this technique is very sensitive to changes in the local and electronic structure of solids after different treatments and can be effectively used to characterize irradiated polymer films.[8–9]

II. EXPERIMENTAL AND CALCULATIONAL DETAILS

The PTES films were produced from alkoxide solutions of phenyltriethysilane $C_6H_5Si(OC_2H_5)_3$ (PTES, Aldrich Chimica, Milan). Water in a molar ratio of 3 H_2O to 1 PTES, and HCl in a molar ratio of 1 HCl to 100 PTES were added to the alkoxide solution. The hydrolysis of ethoxy groups of the PTES alkoxide yields $C_6H_5Si(OH)_3$ molecules, which condense into a three-dimensional siloxane gel. The various solutions were then diluted in order to obtain film thicknesses in the range of 600–1000 nm, which is optimal for irradiation and analysis. The films were irradiated at room temperature with 3-MeV Au^{2+} ions, delivered by the ARAMIS accelerator at the Center de Spectrométrie Nucléaire et de Spectrométrie de Masse[10] under a vacuum of 10^{-7} torr. The ion power was limited to $0.1\ \mathrm{W\,cm^{-2}}$ in order to avoid significant heating of the samples. Ions are neutralized when entering into the siloxane gel.

The carbon $K\alpha$ x-ray emission spectra XES were taken at

 ©1999 The American Physical Society

TABLE I. Observed peaks, VIP's, main AO's, orbital natures (bonding, nonbonding) and functional groups for the XPS VB of PTES (the shift between observed and calculated VIP's is 3.5 eV).

Observed peaks (eV)	VIP's (eV)	Main AO's	Orbital nature	Functional group
24.9	23.95-22.66	O 2s (0.9), Si 3s (0.1)	s_σ (O 2s-Si 3s)-B	O-Si
17.1	20.72-17.92	C 2s	s_σ (C 2s-C 2s)-B	-Ph
14.1	14.91-14.16	C 2s (0.8), Si 3s (0.2)	s_σ (C 2s-Si 3s)-B	C-Si
13.0	12.52	C 2p (0.5), Si 3s (0.5)	p_σ (C 2p-Si 3s)-B	C-Si
9.1	11.71-10.72	O 2p (0.6), Si 3s (0.4)	p_σ (O 2p-Si3s)-B	O-Si
6.6	10.86-10.27	C 2p	p_π (C 2p-C 2p)-B	-Ph
5.1	7.39-5.76	O 2p	p_π (lone pair)-NB	-O-

the Advanced Light Source (Beamline 8.0), employing the University of Tennessee at Knoxville's soft x-ray fluorescence (SXF) endstation.[11] Photons with energies of 310 eV, well above the carbon K absorption edge were delivered to the endstation via the beamline's 89-period, 5-centimeter undulator insertion device and spherical grating monochromator. The carbon $K\alpha$ spectra were obtained with a 600 lines/mm, 10-m radius grating and have an energy resolution between 0.3 and 0.4 eV. The silicon $L_{\mathrm{II,III}}$ XES were measured at Center for Advanced Microstructures and Devices (CAMD) using the Tulane/NIST/Tennessee beamline and 5-m Rowland circle spectrometer with an energy resolution of about 0.5 eV. The silicon $L_{\mathrm{II,III}}$ emission spectra were excited with 110-eV photons, well above the silicon L absorption edge.

The energies of the carbon $K\alpha$ and silicon $L_{\mathrm{II,III}}$ emission spectra were calibrated with reference samples of highly oriented pyrolytic graphite (HOPG) and crystalline silicon.

The x-ray photoelectron spectroscopy (XPS) measurements were taken with a PHI 5600 ci ESCA using monochromatized aluminum $K\alpha$ radiation with 0.3 eV full width at half maximum (FWHM). The energy resolution of the analyzer was 1.5% of the pass energy. We estimate that the energy resolution of the spectrometer is less than 0.35 eV for these XPS measurements. The pressure in the vacuum chamber during these measurements was below 5×10^{-9} mbars. All the measurements were made at room temperature. The XPS spectra were calibrated using the Au $4f_{7/2}$ signal from a gold foil sample. The binding energy for Au $4f_{7/2}$ electrons is 84.0 eV.

The electronic states of PTES were calculated with a deMon density-functional theory (DFT) program[12,13] from a model monomer. For the deMon program we used the maximum number of primitive bases in all combined contractions (3600), contractions (900), orbitals (255), and atoms (45). Optimized Cartesian coordinates from the semi-empirical AM1 method (version 6.0) were used for the geometry of the molecule.[14] The deMon calculations were performed using the B88/P86 exchange-correlation potential, obtained from Becke's 1988 exchange functional[15] and Perdew's 1986 correlation functional.[16] In the program, we used a nonrandom grid and polarized valence double-zeta (DZVP) basis of (621/41/1*) for the carbon and oxygen atoms, (41) for the hydrogen atoms, and (6321/521/1*) for the silicon atoms. Auxiliary fitting functions labeled (4, 4; 4, 4) for the carbon and oxygen atoms, (3, 1; 3, 1) for the hydrogen atoms and (5, 4; 5, 4) for the silicon atoms were utilized. In order to obtain the core-electron binding energies of the carbon 1s, oxygen 1s, and silicon 2p electrons with scaled DZVP bases, we used scaling factors for Gaussian-type orbitals of carbon, oxygen and silicon, provided by Chong and co-workers. For the vertical ionization potentials (VIP's) of the valence regions, we used the restricted diffuse ionization (rDI) model. A superposition of peaks centered on the VIP's, I_k, was constructed to simulate the valence XPS of the theoretical polymer. As is usually done,[17–20] each peak was represented by a Gaussian curve. The intensity of the peaks was estimated from the relative photoionization cross sections for aluminum $K\alpha$ radiation using the Gelius intensity model.[21] Theoretical values from Yeh (Table I), were used for the relative atomic photoionization cross sections.[22] For the linewidth of the models, $WH(k)$, we used $WH(k)=0.10\,I_k$, which is proportional to the ionization energy and has been used in previous work.[17–20] In order to account for solid-state effects, a quantity $W\Delta$ (Refs. 17–20) is subtracted from the computed VIP's and core-electron binding energies (CEBE's). The quantity $W\Delta$ denotes the sum of the work function of the sample, W, and other energy effects (Δ), such as the polarization energy, the width of the intermolecular band formation, and peak broadening in the solid state. For polymers, the experimental $W\Delta s$ can be estimated from differences between the theoretical CEBE's (or VIP's) of monomers or oligomers (corresponding to ''gas phase'' situations), and experimental binding energies of the actual polymer. For polyethylene, for example, a value of 5.3 eV for $W\Delta$ was obtained from a 290.3-eV CEBE of $C_{13}H_{28}$ in a gas phase[23] and a 285.0-eV CEBE for solid polyethylene.[24] In order to compare the calculated VIP's (or CEBE's) for single molecules of the oligomer model with the experimental values of the solid polymer, each computed CEBE (or VIP) I_k' must be shifted by the quantity $W\Delta, I_k(I_{\mathrm{FD}})=I_k'-W\Delta$, to convert to a core-electron binding energy (or ionization energy) $I_k(I_{\mathrm{FL}})$ scale that is relative to the Fermi level.

The XES intensity of the carbon and silicon spectral lines was obtained by summing the squares of the linear combination of atomic-orbital (LCAO) coefficients, $|C_{j[2p(A)]l}|^2$, of the atomic orbitals $\chi_{2p(A)}(r)$ centered on the given carbon and $|C_{j[3s3d(B)]l}|^2$ of the atomic orbitals $\chi_{3s3d(B)}(r)$ centered on the given silicon atoms, where $l=x$, y, and z. Each peakin the theoretical XES spectra is also represented by a Gaussian curve, with the same weight and full width at half maximum

(FWHM = 1.3 eV) as the experimental spectra.

The calculated spectra are compared to experimental x-ray photoelectron valence band (XPS VB) and x-ray emission spectra (carbon $K\alpha$ and silicon $L_{II,III}$), allowing for a detailed analysis of the occupied molecular orbitals of phenyltriethoxysilane.

III. RESULTS AND DISCUSSION

Fluorescent x-ray emission spectroscopy with samples excited near an absorption threshold can be considered a two-step process. The first step corresponds to an electron transition from a core level to an empty valence level when the sample absorbs an incident photon. The second step is the emission of a photon when an electron makes a transition from an occupied valence level to fill the core hole created by the incident photon absorption. Both steps are governed by the dipole selection rule, $\Delta l = \pm 1$, which means that the $1s$ core level holes in carbon and $2p$ holes in silicon can only be filled by $2p$ and $3s3d$ valence electrons, respectively. As the core holes are localized to their particular atoms, the transition matrix elements are dominated by the carbon $2p$ and silicon $3s3d$ contributions from these particular atoms, and as a result all nonlocal contributions to the transition matrix element can be neglected. This allows for the independent measurement of partial carbon $2p$ and silicon $3s3d$ density of states (DOS) distributions for each particular element in the material (carbon and silicon).

In order to compare the valence states measured by XES (site selective and symmetry-restricted DOS) with XPS measurements (total DOS) the location of the top of the valence band (which corresponds to the Fermi level in a metallic system) must be known. In the x-ray emission spectra this energy band corresponds to emissions from occupied outer molecular orbitals. The initial state of a XES is the final state of a XPS. The XES Fermi level can be obtained from the binding energies of corresponding core levels.

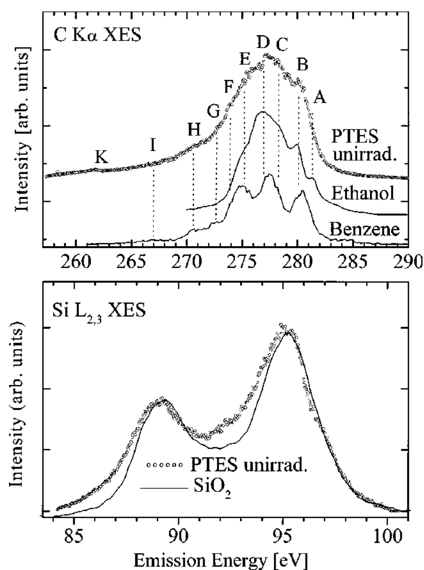

FIG. 1. Carbon Kα XES of unirradiated PTES films and reference compounds.

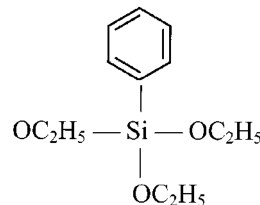

FIG. 2. Chemical structure of phenyltriethoxysilane (PTES).

A. Electronic structure and chemical bonding of unirradiated PTES films

The results of measurements of carbon $K\alpha$ XES of unirradiated phenyltriethoxysilane are presented in Fig. 1. According to the chemical structure of PTES (Fig. 2) there are two inequivalent carbon atom sites located in the phenyl and ethanol side groups. A comparison of the carbon $K\alpha$ XES of PTES with spectra of benzene[25] and ethanol[26] (see Fig. 1) shows that the carbon $K\alpha$ XES of PTES have features that closely resemble those of only benzene monomer because in three-dimensional siloxane gel there is no ethanol and no bonds between carbon and an hydroxide OH.

The silicon $L_{II,III}$ XES of unirradiated PTES films (Fig. 1) shows a two-peaked structure similar to SiO_2.[27] This is expected because the silicon atoms in a siloxane three-dimensional gel are coordinated by two oxygen and one hydroxide side groups via oxygen atoms, and therefore one would expect a dominant silicon-oxygen bonding emission spectrum.

Figure 3 and Tables I–III present a comparison of the experimental and calculated XPS valence band (VB) and XES spectra of PTES. Table I lists the observed XPS VB peaks, the calculated VIP's, the main AO's, the orbital natures and the functional groups of these spectra. The data shows that the low-binding-energy side of the XPS valence band of PTES (0–10 eV) is formed by oxygen $2p$ bonding and nonbonding states and carbon $2p$ bonding states. The peaks of the XPS VB located at 13.0, 14.1, 17.1, and 24.9 eV can be attributed to carbon $2p$ (silicon $3s$), carbon $2s$ (sili-

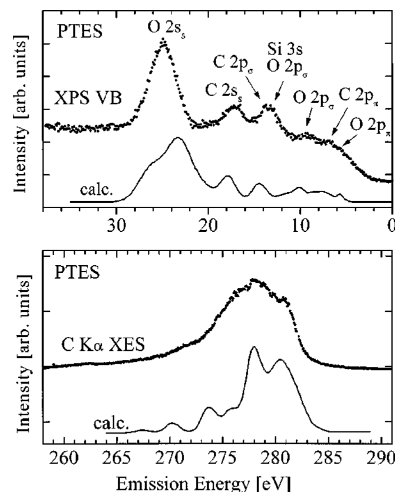

FIG. 3. Experimental and calculated XPS VB and carbon $K\alpha$ XES of unirradiated PTES. The correction of XPS spectra for charging effects is about 12.3 eV.

TABLE II. Observed peaks, orbital natures (bonding, nonbonding), and functional groups for carbon $K\alpha$ XES (the shift between observed and calculated VIP's is 1.0 eV).

Observed peaks (eV)	VIP's (eV)	Main AO's	Orbital nature	Functional group
271-279	274-277	C $2p$ (0.5), Si $3s$ (0.5)	p_σ (C $2p$-Si $3s$)-B	Si-C
276-281	278-284	C $2p$	p_π (C $2p$-C $2p$)-B	-Ph

con $3s$), carbon $2s$ and oxygen $2s$ states, respectively. The intensities of the peaks in the respective energies follow the oxygen, carbon, and silicon content of the system weighted by the atomic photoionization cross sections. The most intense peak located around 24.9 eV corresponds to ionization from s_σ (oxygen $2s$-silicon $3s$) bonding orbitals that are related to the oxygen-silicon (O-Si) functional group. The next group of XPS VB peaks located around 17.1 is due to the s_σ (carbon $2s$-$2s$) bonding orbitals of the phenyl (Ph) group. The peaks located around 14.1 and 13.0 eV are related to s_σ (carbon $2s$-silicon $3s$) and p_π (carbon $2p$-silicon $3s$) bonding orbitals of the carbon-silicon (C-Si) functional groups. The low intensity peak located at 9.1 eV is related to the p_σ (oxygen $2p$-silicon $3s$) bonding orbitals of the oxygen-silicon (O-Si) functional group. The peaks around 6.6 and 5.1 eV are due to p_π (carbon $2p$-carbon $2p$) bonding orbitals, and p_π oxygen $2p$ lone-pair nonbonding orbitals.

Another way to check the validity of the molecular-orbital (MO) calculations is by comparing the experimental and calculated carbon $K\alpha$ and silicon $L_{\mathrm{II,III}}$ x-ray emission spectra of PTES (which probes the distribution of the occupied carbon $2p$ and silicon $3s3d$ states). This comparison is shown in Fig. 3 and Table II for carbon $K\alpha$, showing that the shape of the XES is determined by the p_σ (carbon $2p$-carbon $2p$) and p_π (carbon $2p$-silicon $3s$) bonding orbitals of the phenyl (Ph) and silicon-carbon (S-C) functional groups, respectively. Overall there is reasonable agreement between the experimental and theoretical carbon $K\alpha$ XES. However, the values listed in Table III show that for the silicon $L_{\mathrm{II,III}}$ XES there are some differences between the calculated and experimental spectra. According to the calculations the s_σ (silicon $3s$-oxygen $2s$), p_σ (silicon $3s$-carbon $2p$) and p_σ (silicon $3s$-oxygen $2p$) bonding orbitals of the silicon-oxygen (Si-O), silicon-carbon (Si-O), and silicon-oxygen (Si-O) functional groups, respectively, form the two main peaks of the silicon $L_{\mathrm{II,III}}$ XES, which are separated by about 11.9 eV. The experimental silicon $L_{\mathrm{II,III}}$ XES show a splitting of only about 6.1 eV (Fig. 1). In our spectrometer the energy range of the measured silicon $L_{\mathrm{II,III}}$ XES is restricted by the size of the detector, which for this wavelength is not more than about 16.5 eV. Also, we did not measure the intensity distribution in the region from 70–82 eV, where an additional sub-band related to silicon $3s$-oxygen $2s$ bonding is seen in the spectra of SiO_x. [27] According to reference,[27] the experimental and theoretical silicon $L_{\mathrm{II,III}}$ XES of the silicon-oxygen system contains three sub-bands that are related to silicon $3s$-oxygen $2s$, silicon $3s$-oxygen $2p$, and silicon $3d$-oxygen $2p$ bonding, respectively. We only observe two main sub-bands in our calculated PTES spectrum. The calculated silicon $L_{\mathrm{II,III}}$ XES of PTES is influenced by the accuracy of the values of the valence and core level states. For the calculations of the silicon $2p$ binding energy we have errors on the order of 1.5–2.0 eV with a scaled basis. Considering the molecular size of model monomer, our computer capacity and the calculation times involved, we used a scaled-DZVP basis that may have a maximum error of about 4.0 eV. We used a polarized DZVP basis set for calculating the functions of the atoms involving d functions as polarized functions on the atoms, since the distortion of electron distribution is more strongly pronounced in chemical bonds. However, in our calculations of the PTES dimer molecule, we did not observe a d functional contribution to the chemical bonding on the silicon atoms. Therefore we have observed the same calculation problems with our Si $L_{\mathrm{II,III}}$ XES that have been observed in other silicon-oxygen systems.[27]

B. Local structure of irradiated PTES films

The irradiation of PTES films by Au^{2+} and C^{+} ions modifies the fine structure of the carbon $K\alpha$ XES (Fig. 4). As shown, the irradiation of PTES films by gold ions with doses from 5×10^{14}–$2.5\times10^{15}\,\mathrm{cm}^{-2}$ leads to a smearing of the spectral features, but does not seem to indicate chemical disordering of the system which would be observed in changes to the shape of spectral features. The most dramatic changes to the carbon $K\alpha$ XES are found in the PTES films that were irradiated by carbon ions with doses of $5\times10^{15}\,\mathrm{cm}^{-2}$. Where one observes a decrease in the relative intensity of the high-energy sub-bands (1-2) and the appearance of a low-energy sub-band (6). Based on our MO LCAC calculations of PTES

TABLE III. Observed peaks, orbital natures (bonding, nonbonding), and functional groups for Si $L_{\mathrm{II,III}}$ XES (the shift between observed and calculated VIP's is 0.0 eV).

Observed peaks (eV)	VIP's (eV)	Main AO's	Orbital nature	Functional group
89.1	85.5-87.6	Si $3s$ (0.1), O $2s$ (0.9)	s_σ (Si $3s$-O $2s$)-B	Si-O
91.6	96.7-97.4	Si $3s$ (0.2), C $2s$ (0.8)	s_σ (Si $3s$-C $2s$)-B	Si-C
92.7	99.1-100.0	Si $3s$ (0.5), C $2p$ (0.5)	p_σ (Si $3s$-C $2p$)-B	Si-C
95.2-96.9	100.9-101.6	Si $3s$ (0.4), O $2p$ (0.6)	p_σ (Si $3s$-O $2p$)-B	Si-O

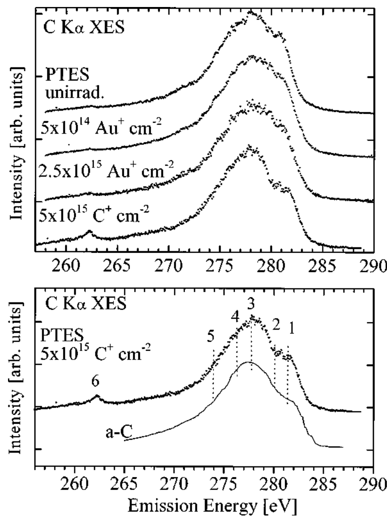

FIG. 4. Carbon $K\alpha$ XES of irradiated PTES films (upper panel) and comparison of spectra of irradiated PTES films and reference compounds (lower panel).

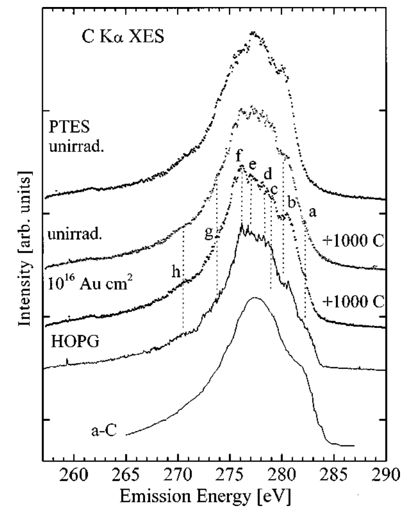

FIG. 6. Carbon $K\alpha$ XES of unirradiated and irradiated PTES films after annealing at 1000 °C.

and comparisons of our carbon $K\alpha$ XES of irradiated PTES films with spectra of reference samples, shown in Fig. 4, one can conclude that irradiation leads to a release of hydrogen from both of the side groups in the molecule, breaking the carbon-hydrogen bonds, and forming amorphous carbon clusters. No new silicon-carbon bonds are formed. For this reason, the carbon $K\alpha$ XES of the PTES film irradiated by carbon ions at a dose of $5\times10^{15}\,\mathrm{cm}^{-2}$ has features that are similar to those in spectra of amorphous carbon (a-C).[28]

The silicon $L_{\mathrm{II,III}}$ XES of irradiated PTES films are presented in Fig. 5. One observes that irradiation of the PTES film with gold ions with doses up to $5\times10^{14}\,\mathrm{cm}^{-2}$ does not significantly change the general shape of the silicon $L_{\mathrm{II,III}}$ XES. Increasing the dose to $2.5\times10^{15}\,\mathrm{cm}^{-2}$ rearranges the silicon $L_{\mathrm{II,III}}$ XES fine structure of the irradiated PTES film, which now consists of five overlapping sub-bands (1-5) (Fig. 5). Features 1 and 4 and 2 and 5 closely resemble the main maxima of the silicon $L_{\mathrm{II,III}}$ XES of SiC and SiO_2, respectively. This is direct spectroscopic evidence for the conversion of the polymer into an amorphous Si:O:C ceramic with the formation of silicon-carbon and silicon-oxygen bonds. Feature 3 closely resembles the intensity maximum of the silicon $L_{\mathrm{II,III}}$ XES of crystalline silicon (c-Si) which can be due to the formation of unpaired Si bonds and Si-Si bonds because of the atomic disordering produced by nuclear collisions. In principle it can be also a result of the precipitation of silicon nanoparticles induced by the ion irradiation but no photoluminescence is fixed in this case. The precipitation of Si nanoparticles was observed in earlier XES measurements of semiconducting Si_3N_4 and SiO_2 films induced by excimer laser and electron beam irradiation.[29,30,7]

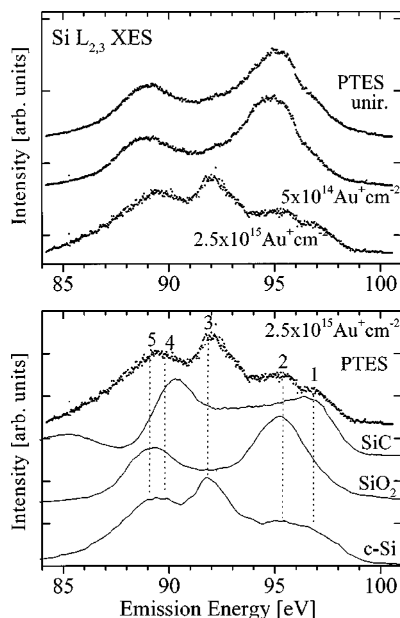

FIG. 5. Silicon $L_{\mathrm{II,III}}$ XES of irradiated PTES films (upper panel) and comparison of spectra of irradiated PTES films and reference compounds (lower panel).

C. Compositional and structural changes during annealing

Figure 6 displays the measurements of carbon $K\alpha$ XES of PTES films after annealing at 1000 °C, and after combined treatments of irradiation and annealing. One observes that the annealing of the unirradiated PTES films modifies the fine structure of the carbon $K\alpha$ XES, revealing some spectral features that are typical for spectra of sp^2 hybridized graphite (see Fig. 6). This means that the proportion of sp^2 hybridization of the carbon atoms increases with respect to the unannealed films. The combined treatment of PTES films leads to spectra that are even more similar to the carbon $K\alpha$ XES of graphite, and is in a good agreement with XPS measurements (see Fig. 7). The charging effects in the XPS carbon $1s$ level and VB level spectra typical for unirradiated PTES insulated samples is reduced after combined treatment due to the segregation of carbon atoms into graphitelike clusters. Therefore one can conclude that the proportion of sp^2 hybridization is higher after the combined treatment than after annealing alone of the PTES film. In Fig. 7 one observes a small peak in the XPS carbon $1s$ level at 302 eV in the spectrum of the unirradiated PTES film. This is an indication of the existence of π bonding in the system. After irradiation the double peaked structure of the XPS of the carbon $1s$

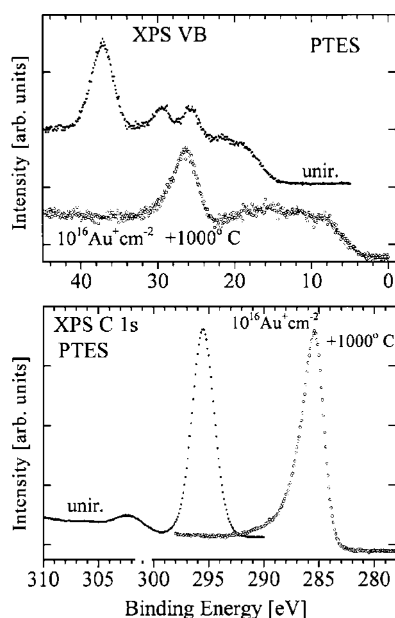

FIG. 7. XPS of the carbon 1s and VB levels of unirradiated and irradiated PTES films after annealing at 1000 °C.

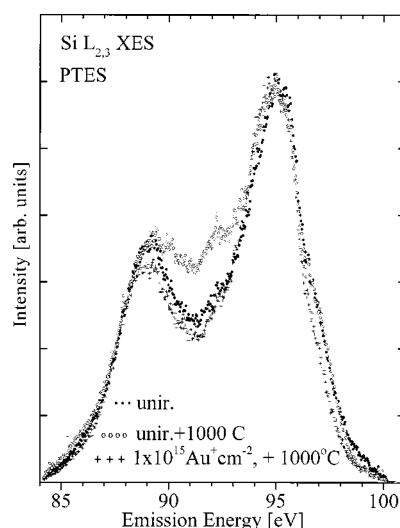

FIG. 8. Silicon $L_{II,III}$ XES of unirradiated and irradiated PTES films after annealing at 1000 °C.

level disappeared. The line shape of the XPS carbon 1s level of the irradiated PTES films becomes slightly asymmetric, typical of a Doniach-Sunjic profile, indicating the existence of charge carriers at the Fermi level found in conducting samples, whereas the other profile is more Lorentizian, which is typical for insulating samples. The XPS VB levels of the irradiated PTES films show a smearing and broadening of band peaks, showing that the structural order is being destroyed.

Silicon $L_{II,III}$ XES measurements of the annealed PTES films are presented in Fig. 8. One observes that annealing of the unirradiated PTES film changes the intensity distribution with respect to that of the unannealed film or film after the combined treatment. Unirradiated film cracks a flake off when the specimen is directly annealed and some contribution of Si substrate is fixed in silicon $L_{II,III}$ XES.

D. Chemical bonding and hardness of irradiated and annealed PTES films

In addition to the structural and compositional conversion of irradiated polymer films into amorphous composite ceramics, the irradiation treatment increases the hardness of the films beyond the hardness of typical ceramics coatings. The hardness of deposited PTES films is on the order of organic polymers (about 0.35 GPA).[31] When the samples are saturated by irradiation the hardness of the samples is on the order of two times higher than that of pure silica (10 ± 0.5 GPa). The hardness of these films is also significantly higher than the hardness of Si:O:C amorphous films deposited by cosputtering of silica and carbon.[31] This makes irradiated organic-inorganic polymer films attractive for a variety of applications that might benefit from hard, insulating materials.

Our XES measurements show that carbon clusters formed during irradiation of the PTES films are similar to those in amorphous carbon (Fig. 2) with about 20% sp^3 hybridization, with less tendency to rearrange into turbostatic (graphitelike) carbon than direct thermal treatments (Fig. 6). One can conclude that the diamondlike clusters that are formed during irradiation enhance the hardness of the PTES films. When the irradiated films are annealed the carbon clusters formed by the radiolysis of phenyl rings do not retain the diamondlike clusters, and the hardness decreases by about 15%.[31]

IV. CONCLUSION

We have studied the electronic structure and chemical bonding of phenyltriethysilane $C_6H_5Si(OC_2H_5)_3$ PTES films with x-ray emission and photoelectron spectroscopies and deMon MO LCAO calculations. The experimental and theoretical spectra are in good agreement. We found that irradiation with gold and carbon ions changes the composition and chemical structures of PTES films. Based on our x-ray fluorescence measurements we conclude that at ion doses higher than $5\times10^{14}\,\mathrm{cm}^{-2}$ the conversion of the PTES polymer into a Si:O:C ceramic occurs.

ACKNOWLEDGMENTS

The authors are greatly thankful to Dr. J.-C. Pivin for preparation of the samples and discussion. This work was supported by the Russian Science Foundation for Fundamental Research (Project Nos. 96-15-96598 and 99-03-32503), a NATO Linkage Grant (No. HTECH.LG 971222), INTAS-RFBR (95-0565), NSF Grant Nos. DMR-901 7997 and DMR-9420425, and the DOE EPSCOR and Louisiana Education Quality Special Fund DOE-LEQSF (1993-95-03). Research at the Advanced Light Source at Lawrence Berkeley National Laboratory was supported by the U.S. Department of Energy (DE-AC03-76SF00098).

[1] C. J. Brinker and G. W. Scherer, in *Sol-gel Science: The Physics and Chemistry of Sol-gel Processing* (Academic, Boston, MA, 1990), p. 787.
[2] C.-J. Chu, G. D. Soraru, F. Bobanneau, and J. D. Mackenzie, in *Amorphous and Crystalline Silicon Carbide and Related Materials II*, edited by M. M. Rahman and G. L. Harris, Springer Proceedings in Physics Vol. 43 (Springer, Heidelberg, 1989), p. 66.
[3] J. C. Pivin and P. Colombo, Nucl. Instrum. Methods Phys. Res. B **120**, 262 (1996).
[4] E. Z. Kurmaev, V. R. Galakhov, S. N. Shamin, V. I. Sokolov, M. H. Ludwig, and R. E. Hummel, J. Phys.: Condens. Matter **9**, 2671 (1997).
[5] E. Z. Kurmaev, A. V. Ezhov, S. N. Shamin, V. M. Cherkashenko, Yu. G. Andreev, and T. Lundstrom, J. Alloys Compd. **248**, 86 (1997).
[6] E. Z. Kurmaev, S. Stadler, D. L. Ederer, Yu. M. Yarmoshenko, D. A. Zatsepin, M. Neumann, T. A. Callcott, M. M. Grush, R. C. C. Perera, S. E. Danilov, and V. L. Arbuzov, Mater. Trans., JIM **39**, 570 (1998).
[7] E. Z. Kurmaev, S. N. Shamin, V. R. Galakhov, A. A. Makhnev, M. M. Kirillova, T. E. Kurennykh, V. B. Vykhodets, and S. Kaschieva, J. Phys.: Condens. Matter **9**, 6969 (1997).
[8] R. P. Winarski, D. L. Ederer, J.-C. Pivin, E. Z. Kurmaev, S. N. Shamin, A. Moewes, G. S. Chang, C. N. Whang, K. Endo, and T. Ida, Nucl. Instrum. Methods Phys. Res. B **145**, 401 (1998).
[9] E. Z. Kurmaev, D. A. Zatsepin, R. P. Winarski, S. Stadler, D. L. Ederer, A. Moewes, V. V. Fedorenko, S. N. Shamin, V. R. Galakhov, G. S. Chang, and C. N. Whang, J. Vac. Sci. Technol. A **17**, 593 (1999).
[10] E. Cotterau, J. Camplan, J. Chaumont, R. Meunier, and H. Bernas, Nucl. Instrum. Methods Phys. Res. B **45**, 293 (1990).
[11] J. J. Jia, T. A. Callcott, J. Yurkas, A. W. Ellis, F. J. Himpsel, M. G. Samant, J. Stöhr, D. L. Ederer, and R. C. C. Perera, Rev. Sci. Instrum. **66**, 1394 (1995).
[12] A. St-Amant, D. R. Salahub, Chem. Phys. Lett. **169**, 387 (1990).
[13] A. St-Amant, Ph.D. thesis, University of Montreal, 1991.
[14] M. J. S. Dewar and E. G. Zoebisch, THEOCHEM **180**, 1 (1988); M. J. S. Dewar, E. G. Zoebisch, E. F. Healy, and J. J. P. Stewart, J. Am. Chem. Soc. **107**, 3902 (1985).
[15] A. D. Becke, Phys. Rev. A **38**, 3098 (1988).
[16] J. P. Perdew, Phys. Rev. B **33**, 8822 (1986).
[17] K. Endo, Y. Kaneda, M. Aida, and D. P. Chong, J. Phys. Chem. Solids **66**, 1131 (1995).
[18] M. Aida, Y. Kaneda, N. Kobayashi, K. Endo, and D. P. Chong, Bull. Chem. Soc. Jpn. **67**, 2972 (1994).
[19] K. Endo, C. Inoue, Y. Kaneda, M. Aida, N. Kobayashi, D. P. Chong, Bull. Chem. Soc. Jpn. **68**, 528 (1995).
[20] K. Endo, Y. Kaneda, H. Okada, D. P. Chong, and P. Duffy, J. Phys. Chem. **100**, 19 455 (1996).
[21] U. Gelius and K. Siegbahn, Faraday Discuss. Chem. Soc. **54**, 257 (1972); U. Gelius, J. Electron Spectrosc. Relat. Phenom. **5**, 985 (1974).
[22] J.-J. Yeh, *Atomic Calculation of Photoionization Cross Section and Asymmetry Parameters* (Gordon and Breach, New York, 1993).
[23] J. J. Pireaux, S. Svensson, E. Basilier, P. A. Malmqvist, U. Gelius, R. Caudana, and K. Siegbahn, Phys. Rev. B **14**, 2133 (1976).
[24] G. Beamson and D. Briggs, in *High Resolution XPS of Organic Polymers*, The Science ESCA 3000 Database (Wiley, Chichester, 1992).
[25] P. Skytt, J. Guo, N. Wassdahl, J. Nordgren, Y. Luo, and H. Agren, Phys. Rev. A **52**, 3572 (1995).
[26] K. Gunnelin, M. Wirde, D. Bylund, and G. Bray (unpublished).
[27] G. Wiech, H.-O. Feldhutter, and A. Simunek, Phys. Rev. B **47**, 6981 (1993).
[28] E. Z. Kurmaev, S. N. Shamin, S. V. Shulepov, and K. M. Kolobova, Carbon **24**, 249 (1986).
[29] E. Z. Kurmaev, S. N. Shamin, V. E. Dolgih, K. Kurosawa, K. Nakamae, Y. Takigawa, A. Kameyama, A. Yokotani, and W. Sasaki, Jpn. J. Appl. Phys., Part 2 **33**, L1549 (1994).
[30] K. Kurosawa, P. R. Herman, E. Z. Kurmaev, S. N. Shamin, V. R. Galakhov, Y. Takigawa, A. Yokotani, A. Kameyama, and W. Sasaki, Appl. Surf. Sci. **126**, 83 (1998).
[31] J.-C. Pivin and P. Colombo, J. Mater. Sci. **32**, 6163 (1997); **32**, 6175 (1997).